Materials Today Communications 32 (2022) 103996

Contents lists available at ScienceDirect

Materials Today Communications

journal homepage: www.elsevier.com/locate/mtcomm

The magnetic properties prediction and composition design of La-Co substitution Sr-hexaferrite based on high-through experiments and machine learning

Ruoshui Liu [a,b,c], Lichen Wang [b,f], Zhiyi Xu [b,c], Ciyu Qin [a,b], Ziyu Li [a,b], Xiang Yu [b,c], Dan Liu [d], Huayang Gong [b], Tongyun Zhao [b,c], Jirong Sun [c], Fengxia Hu [c], Baogen Shen [a,b,c,e,f,*]

[a] School of Rare Earths, University of Science and Technology of China, Hefei, Anhui 230026, China
[b] Ganjiang Innovation Academy, Chinese Academy of Sciences, Ganzhou, Jiangxi 341119, China
[c] Beijing National Laboratory for Condensed Matter Physics, Institute of Physics, Chinese Academy of Sciences, Beijing 100190, China
[d] Department of Physics, School of Artificial Intelligence, Beijing Technology and Business University, Beijing 100048, China
[e] Ningbo Institute of Materials Technology & Engineering, Chinses Academy of Sciences, Ningbo, Zhejiang 315201, China
[f] Innovation Center for Applied Magnetics of Zhejiang Province, Ningbo, Zhejiang 315201, China

ARTICLE INFO

Keywords:
La-Co substitution Sr-hexaferrite
Magnetic Properties
Composition design
Machine learning technique
Nature-inspired algorithm

ABSTRACT

La-Co co-substitution is an effective method to improve the magnetic properties of Sr-hexaferrite but knowing the most suitable substitution amount requires many trial and error experiments. Combining high-throughput experiments with machine learning techniques is a promising way to quickly realize the composition design. With that in mind, we adopted three frequently-used machine learning models, namely Gaussian process regression (GPR), support vector regression (SVR), and radial basis function network (RBFN) as candidate prediction models to learn the 145 samples accumulated from the high-throughput experiments. Furthermore, three nature-inspired algorithms called particle swarm optimization (PSO), genetic algorithm (GA), and grey wolf algorithm (GWA) were applied to search for the optimal combination of the hyper-parameters, improving the performance of the machine learning models. To compare the accuracy of these models and simultaneously validate the experimental data's reliability, the 20 samples under the same experimental conditions obtained from literature were selected as the testing data. The comparison results showed that the SVR model with the GWA algorithm (SVR-GWA) performed better than the other methods. After that, the predicted figures of saturation magnetization (M_S) and coercivity (H_{cJ}) were obtained by the SVR-GWA model. Moreover, five compositions not involved in training and testing data were randomly selected from the prediction figures to further verify the reliability of the SVR-GWA model, which achieves the goal of fast and accurate composition design of La-Co substitution Sr-hexaferrite.

1. Introduction

Due to the rapid expansion of electric vehicle and wind power industries presently, permanent magnets become important technologically and commercially, and constant research and development efforts are promoted from the foundation. Since the discovery of barium ferrite ($BaFe_{12}O_{19}$) in the 1950s [1], there has been an increasing degree of interest in the M-type hexagonal ferrites, which have high coercivity (H_{cJ}), saturation magnetization (M_S), and Curie temperature, good chemical stability, and simple preparation process [2]. Coupled with the high price of other permanent magnets caused by the scarcity of rare earth elements, hexagonal ferrites have a low cost and richer source of raw materials [3]. There are five crystallographically inequivalent Fe sites, 2*a*, 2*b*, 4f_1, 4f_2, and 12*k*, with moments of 5 μ_B for high-spin Fe^{3+} (d^5) at the majority-spin sites (2*a*, 2*b*, and 12*k*), and those at the minority-spin sites (4f_1 and 4f_2) are coupled in an antiparallel manner along the c-axis, resulting in a ferrimagnetic structure with a saturation moment of 20 μ_B per formula unit (f.u.) in the ground state. The simultaneous substitution of La and Co in M-type Sr-hexaferrite (will be denoted by La-Co SrM) resulted in marked improvement in the magnetic performance [4], which is the only commercial ferrite magnets produced by Hitachi [5] and TDK [6]. Nowadays, several investigations

* Corresponding author at: School of Rare Earths, University of Science and Technology of China, Hefei, Anhui 230026, China.
E-mail address: shenbg@iphy.ac.cn (B. Shen).

https://doi.org/10.1016/j.mtcomm.2022.103996
Received 6 February 2022; Received in revised form 5 July 2022; Accepted 10 July 2022
Available online 14 July 2022

consider the improvement of these La-Co SrM, mainly focusing on Ca-doping by different synthesis methods [7–10], changes in microstructure and morphology [11–13], occupancy distribution of Co ions [14–17], and so on.

However, with increasing variables as the change of these conditions, the number of potential compositions with targeted properties to explore is too large for the traditional method based on trial and error, which is both time-consuming and costly. The computational approach in this connection is of inspiration to solve this problem by using machine learning (ML) tools. As the fourth scientific paradigm of materials science [18], ML has become important means of realizing materials design efficiently. It learns rules and laws from a large amount of experimental data, to build the complex relationships between performance, composition, structure and process, and finally assist guidance of experiments, which greatly saves time and cost. But such efficient data analytics has been very rare in the research of hexaferrite, there are only three related studies so far. I. Kucuk [19] and H. Sozeri [20] used neural network models to predict the hysteresis loop and XRD phase identification respectively of La substituted Ba-hexaferrite prepared from ammonium nitrate melt. T. Pourashraf [21] prepared 17 different ion-substituted ferrites by self-combustion sol-gel method and used an optimized support vector regression (SVR) model to predict remanence (B_r) and coercivity (H_{cJ}). These cases have achieved great success in some performance prediction of hexaferrite, but all of them are based on a single ML model. Based on the theory and characteristics, the performance of the ML model is greatly affected by hyper-parameters and different ML models have different adaptability to different types of data. To this end, it is in urgent need of applying different ML models to search for the most suitable one with a suitable combination of hyper-parameters for a set of specific data.

According to the above analysis, three frequently-used ML models (GPR, SVR, RBFN) and three nature-inspired algorithms (PSO, GA, GWA) are adopted simultaneously in this work to find the better-performed method for composition design of La-Co SrM. It should be noted that nature-inspired algorithms are applied to search for the optimal combination of the hyper-parameters to improve the prediction accuracy of the ML models. And then, the predicted figures of magnetic properties will be established based on the most suitable method for guiding the composition design of La-Co SrM.

With the purpose of efficient and accurate composition design of La-Co SrM based on ML, the remainder of this paper is organized as follows. The experimental process, theory of ML models and nature-inspired algorithms, and workflow of this study are introduced in Section 2. Section 3 shows the training, validation, comparison, and application of the proposed composition design ML methods for La-Co SrM. In Section 4, the specific conclusions of this study and prospects for future work are discussed.

2. Methods

2.1. Experimental and prediction model

This paper adopts the methodology of combining high-throughput experiments and machine learning. As an important part of materials genomics technology, high-throughput experiments are to complete the preparation and characterization of a large number of samples in a short time [22]. Its core is changing the sequential iterative method used in traditional materials research to parallel processing to cause qualitative changes in material research efficiency. The advantage of combining high-throughput experiments with ML is that the former can provide massive basic data for the latter, at the same time provide experimental verification for calculation results, so that the calculation model can be optimized and corrected. It could reduce the cost of manpower and material resources in industrial development and shorten the research period.

To achieve the proposed objectives of this study, focusing on the material composition of M-type ferrites, the predictive power of ML models on the magnetic properties of these ferrites was investigated. For this purpose, the starting materials were industrial grade with $SrCO_3$ (97 %), Fe_2O_3 (99.9 %), La_2O_3 (99 %), and Co_2O_3 (70 %). SrM ferrite of composition $Sr_{1-x}La_xFe_{12-y}Co_yO_{19}$ designed in orthogonal experimental method, were prepared by a solid-state reaction method (defined $x = y = 0$ as pure sample). Stoichiometric mixtures of oxides were thoroughly ground in a ball mill, then calcined in corundum crucibles for 2 h in the air at 1250 °C. The hexaferrite structure was checked by the X-ray diffraction (XRD) technique. The XRD results revealed that the homogeneous phase of M-type Sr-hexaferrite was obtained. And the hysteresis loops of powders were measured at room temperature by using a vibrating sample magnetometer (SQUID-VSM). The whole experimental process is shown in Fig. 1.

Before machine learning, we need to preprocess the experimental data. With the La-Co substitution amount changing, the ratio of Sr and Fe also changed, as the raw material purity of $SrCO_3$ and Fe_2O_3 was different. Therefore, we set the independent variable $\boldsymbol{X}$ of this prediction model to the percentage content of each raw material. As Fig. 2 shows, we screened 145 sets of data containing compositions as well as performances at the temperature of 1250 ℃. The four independent variables $\boldsymbol{X} = (X_1, X_2, X_3, X_4)$ are listed in Table 1, and the corresponding magnetic properties i.e., saturation magnetization (M_S) and intrinsic coercivity (H_{cJ}) of each data are used as the output value $\boldsymbol{Y}$. We use machine learning methods to get two properties ($\boldsymbol{Y} = M_S$ and $\boldsymbol{Y} = H_{cJ}$), that is, finding the relationship of $\boldsymbol{Y} = f(\boldsymbol{X})$.

2.2. Machine learning model

In general, different models have different adaptability to different types of data. With that in mind, three frequently-used classic machine learning models, namely Gaussian process regression (GPR), support vector regression (SVR), and radial basis function network (RBFN) are chosen for comparing the suitability of this type of sample.

2.2.1. GPR

Gaussian process regression (GPR) model [23] also called the Kriging model is an interpolation model, which uses Gaussian process controlled by covariance to generate continuous function. Meanwhile, GPR is an unbiased estimation model with uncertainty but its prediction error is minimized by optimizing hyper-parameters. For an individual x in a training sample $\boldsymbol{x}^{(i)}$ ($i = 1, 2, \ldots, n$), GPR supposes that the objective value satisfies the normal distribution with mean value μ and standard deviation σ^2 defined as:

$$\boldsymbol{Y} = \left[Y\left(x^{(1)}\right), Y\left(x^{(2)}\right), \ldots, Y\left(x^{(n)}\right)\right] \tag{1}$$

The relationship between two individuals in $\boldsymbol{Y}$ is as follows:

$$cov\left[Y\left(x^{(i)}\right), Y\left(x^{(j)}\right)\right] = \sigma^2 \boldsymbol{R}\left[R\left(x^{(i)}, x^{(j)}\right)\right] (i = 1, 2, \ldots, n) \tag{2}$$

Where $\boldsymbol{R}$ is a symmetric correlation matrix; n is the number of samples; R

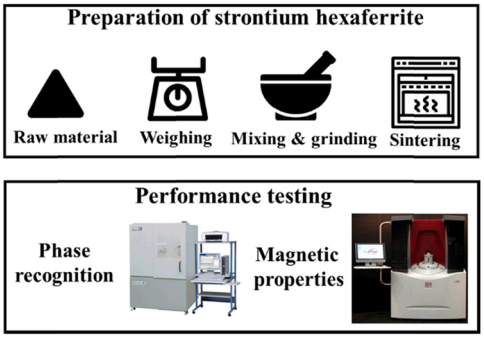

Fig. 1. High-throughput experimental procedure.

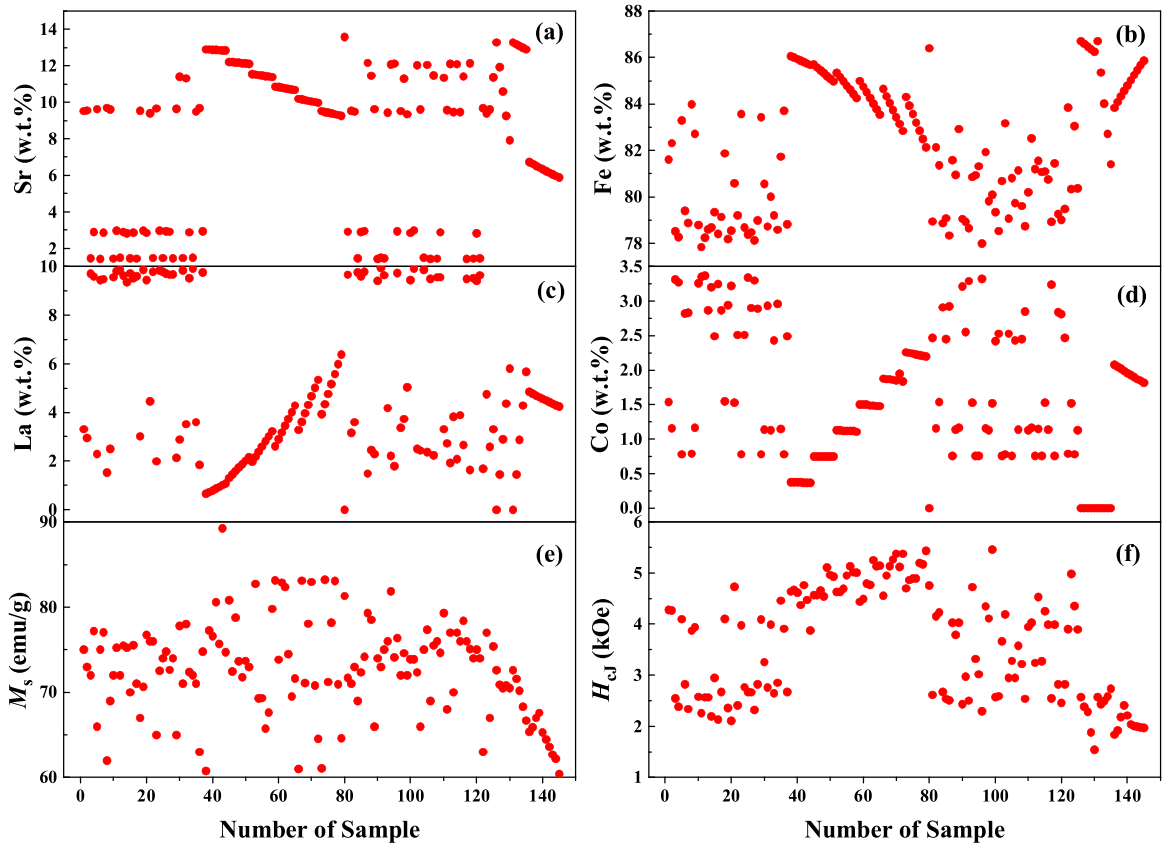

Fig. 2. The statistic of compositions (Sr, Fe, La, and Co) and magnetic properties (M_s and H_{cJ}) of 145 La-Co substitution Sr-hexaferrite sets of data from high-through experiments for training set: (a) content of Sr; (b) content of Fe; (c) content of La; (d) content of Co; (e) M_s; (f) H_{cJ}.

Table 1
Four independent variables $X = (X_1, X_2, X_3, X_4)$ of ML models.

Notation	Description
X_1	Mass fraction of Strontium Carbonate (wt. %)
X_2	Mass fraction of Iron oxide (wt. %)
X_3	Mass fraction of Lanthanum Oxide (wt. %)
X_4	Mass fraction of Cobalt Oxide (wt. %)

is the correlation Gaussian kernel function between two individuals as follows:

$$R\left(x^{(i)}, x^{(j)}\right) = exp\left[-\sum_{k=1}^{ndv} \theta_k \left|x_k^i - x_k^j\right|^{P_k}\right] \tag{3}$$

Where *ndv* is the number of design variables; θ and p are the hyper-parameters; $|x_k^i - x_k^j|$ is the distance between two individuals in the direction of the kth design variable.

The maximum likelihood estimation of the real objective value $\boldsymbol{Y}(\boldsymbol{x})$ is used to find the statistic-parameters μ and σ^2, and the mathematical form is as follows:

$$\ln(L(Y)) = -\frac{n}{2}\ln\left(\sigma^2\right) - \frac{n}{2}\ln(|\boldsymbol{R}|) - \frac{(\boldsymbol{y} - \boldsymbol{1}u)^T \boldsymbol{R}^{-1}(y - \boldsymbol{1}u)}{2\sigma^2} \tag{4}$$

Where $\boldsymbol{1}$ represents the column vector of ones; L represents the maximum likelihood estimation. The GPR model is established once the μ and σ^2 are obtained. Fig. 3 vividly shows the principle of the GPR model.

2.2.2. SVR

Support vector regression (SVR) is to use the SVM (support vector machine) algorithm to find a regression plane so that all the data are the closest to the plane. In this way, the SVR model can be used for linear/non-linear classification and regression, has low generalization error and computational complexity, and can solve high-dimensional problems. The mathematic form of the SVR model is as follows:

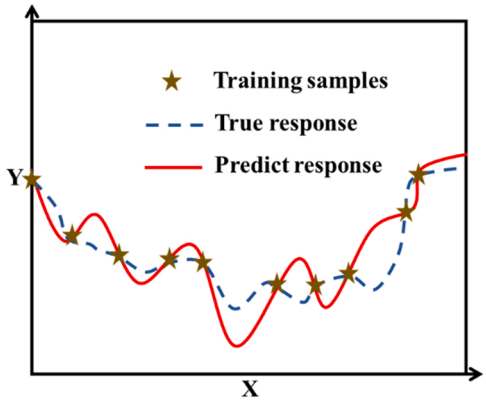

Fig. 3. Diagram of GPR model.

$$\hat{y}\left(\underline{x}\right) = \sum_{k=1}^{N_S} \alpha_k K\left(\underline{x}_k, \underline{x}\right) + b \tag{5}$$

Where: b and α_k are the scalar parameters during the training procedure; $K(\underline{x}_k, \underline{x})$ is the kernel function. The detailed theory and training process of the SVR model are as described previously [24]. It is worth mentioning that the accuracy of the SVR model is highly dependent on the choice of the kernel function. The performance of the SVR model is

highly affected by the kernel function parameter γ and penalty factor c. To better understand the principle of the SVR model, Fig. 4 vividly shows the geometric principle of the SVR model.

2.2.3. RBFN

Radial basis function network (RBFN) [25] is one of the simple training and fast learning convergence machine learning model which can evaluate most nonlinear relationships with relatively high precision. Due to the low computational complexity, the RBFN model is chosen as one of the machine learning models in this study. And then, the evaluation accuracy of the RBFN model is highly affected by the two hyper-parameters, variance σ and the weight coefficient vector ω. To vividly visualize the structure of the RBFN model, Fig. 5 displays the specific schematic diagram.

According to the above discussion, hyper-parameters play an essential role in the evaluation accuracy of these models. For this purpose, the statistic of the hyper-parameters which need to be optimized are shown in Table 2.

2.3. Optimization algorithm

One of the most essential aspects of applying machine learning methods is to establish the model with adequate accuracy and efficiency. Meanwhile, the hyper-parameters of the machine learning model directly determine the performance and prediction accuracy of the model. To address this issue, searching for the suitable hyper-parameters of the machine learning model is the promising way. The appropriate combination of hyper-parameters can significantly improve the prediction accuracy of the model. Therefore, the heuristics intelligent algorithms which can achieve global optimal search are applied in this study to find the hyper-parameters and improve the prediction accuracy of machine learning models. Nevertheless, the same as the machine learning models, different algorithms have different adaptability. To this end, three frequently-used algorithms, namely particle swarm optimization (PSO), genetic algorithm (GA), and grey wolf optimizer (GWO) are adopted as the optimizer.

2.3.1. PSO

The particle swarm optimization (PSO) algorithm [26] is an optimization algorithm based on swarm intelligence, which is characterized by fewer parameters, easy implementation and fast convergence. For an optimization problem, the PSO algorithm obtains the optimal solution through iterative steps. The basic idea is to regard each solution as the position of a particle in the searching space, and each iterative solution process as a motion of particle swarm in the searching space. To show the iteration process more vividly, the typical trajectory of a particle concerning the velocity and position of the particles in the PSO algorithm is displayed in Fig. 6. It is worth mentioning that the specific

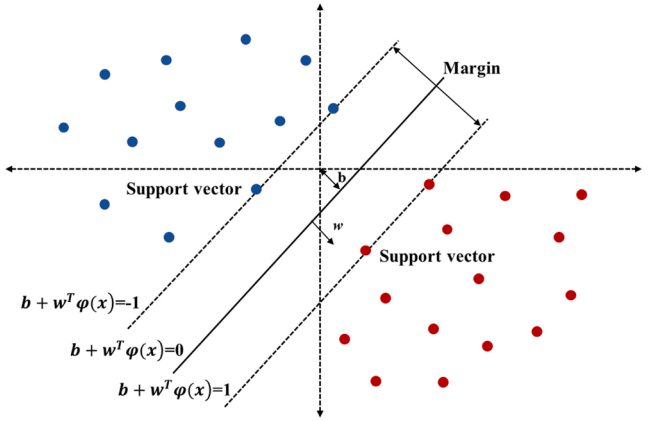

Fig. 4. The diagram of the SVR model.

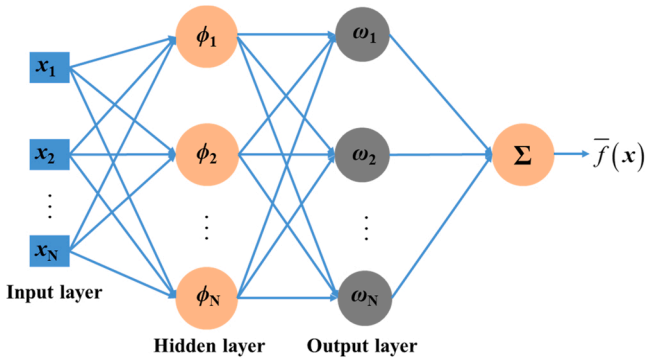

Fig. 5. The structure of the RBFN model.

Table 2
The hyper-parameters for optimization of the models.

Model	Hyper-parameter one	Hyper-parameter two
GPR	θ	p
SVR	γ	c
RBFN	σ	ω

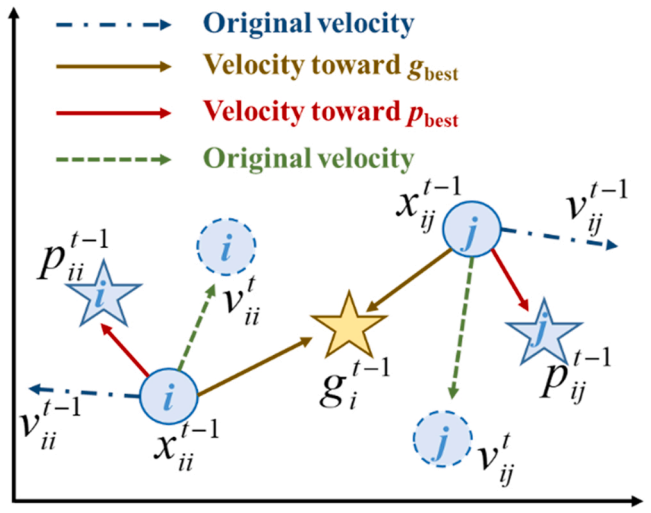

Fig. 6. Typical trajectory of a particle with respect to the velocity and position of the particles in the PSO algorithm.

algorithm parameters adopted in the PSO algorithm are displayed in Table 3.

2.3.2. GA

The genetic algorithm (GA) is an algorithm born regarding the principle of survival of the fittest in nature [27]. According to the principle of survival of the fittest, the GA algorithm evolves generation by generation to produce better and better approximate solutions through replication, crossover and mutation. The genetic algorithm can optimize the search range, has strong global searchability, and does not

Table 3
Specific parameters of the PSO algorithm.

Parameters	Value
Size of the population (m)	50
Number of iterations	100
Weight parameter (ω)	0.8
Acceleration constants (c_1, c_2)	1.8
Maximum velocity of the particle (V_{max})	1

have too many constraints and rules. In general, there are three main steps called crossover, mutation, and selection in GA. The specific diagram and parameters of the GA are displayed in Fig. 7 and Table 4.

2.3.3. GWA

The grey wolf algorithm (GWA) [28] was introduced to optimize the hyper-parameters of these three models. In the GWA, the best solution is the α wolf, the second-best is the β wolf, the third-best is the γ wolf, and the other solutions are δ wolves. During the searching process, α, β, and γ wolves lead the search for the optimal solution. When the stop condition is achieved, the α wolf is output as the best solution. The encircling prey behavior of the wolves is described in Fig. 8. The related parameters of the GWA are shown in Table 5. At the beginning of the iteration of these three algorithms, the initial solutions are randomly generated by the Latin hypercube sampling (LHS).

2.4. Workflow of this paper

According to the three ML models and three algorithms, there are 9 combinations of models and algorithms named as GPR-PSO, GPR-GA, GPR-GWA, SVR-PSO, SVR-GA, SVR-GWA, RBFN-PSO, RBFN-GA, and RBFN-GWA. The scheme of using machine learning technology to establish a material performance prediction model is shown in Fig. 9. First, we sorted out all the experimental data according to Table 1. As shown in Fig. 2, this dataset measured 4 features of each 145 samples. Next, the regression analysis was performed using GPR, SVR, and RBFN algorithms, and the models were optimized by PSO, GA, and GWA, thus we got 9 methods. The 20 sets of data collected from the literature were subjected to validation. Then the model with the smaller MAE, MRE and RMSE, and larger R^2 was selected as our prediction model, which can realize predicting performance value by inputting a certain variable. Finally, performance (H_{cJ} and M_S) prediction images are obtained with two dimensions——La content and Co content.

3. Results and discussion

In this section, the characteristics of La-Co SrM samples were analyzed by the Pearson correlation. And then, using Python program and the core code of Scikit-learn to implement the 9 methods established and validated by 145 experimental samples and 20 literature samples, respectively. After that, the composition design with specific magnetic properties (M_S and H_{cJ}) of La-Co SrM was conducted.

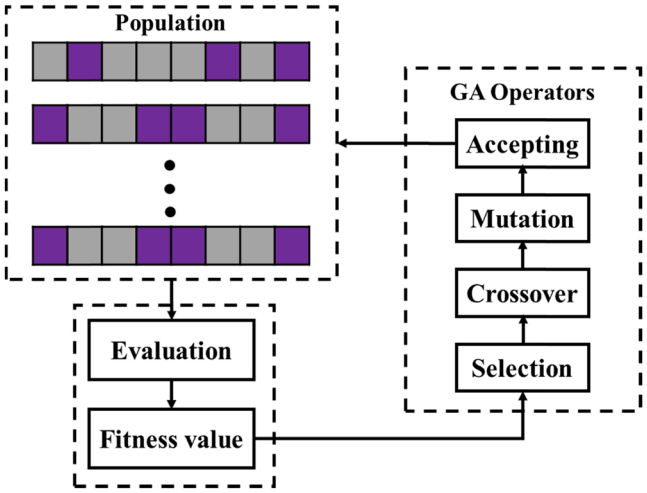

Fig. 7. Optimization process of GA.

Table 4
Parameters used in the GA algorithm.

Parameters	Value
Size of the population (m)	50
Number of iterations	100
Mutative probability	0.005
Cross probability	0.65

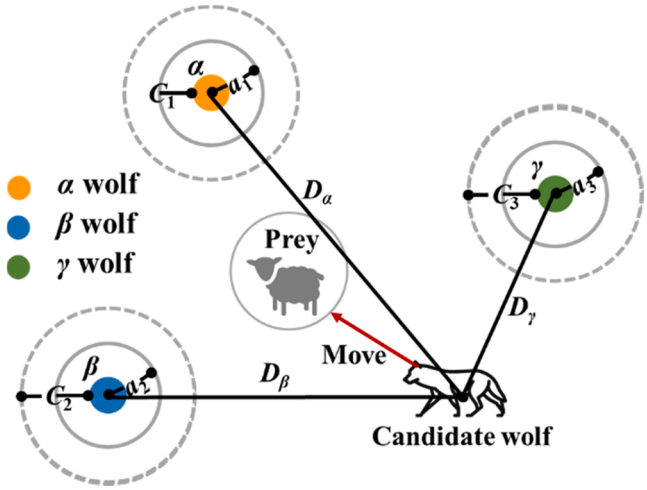

Fig. 8. Optimization process of GWA.

Table 5
Parameters used in the GWA algorithm.

Parameters	Value
Size of the population (m)	50
Number of iterations	100
Synergy coefficient vector A	Rand (−2,2)
Synergy coefficient vector C	Rand (0,2)
Max-step	1

3.1. Correlation analysis of the composition

Pearson correlation coefficient is used to measure the linear correlation between two variables X and Y as formula (6) shows. The value range is between −1 and 1. −1 means complete negative correlation, while +1 means complete positive correlation and 0 means no linear correlation. In other words, the greater the absolute value, the stronger the correlation [29]. But the Pearson correlation coefficient has an obvious defect in that it is only sensitive to linear relationships. If the relationship is non-linear, even if there is a one-to-one correspondence between the two variables, it may be close to 0. Fig. 10 is the correlation histogram between every variable including 4 independent variables and 2 dependent variables in our samples, which are in line with previous experience.

$$\rho_{x,y} = corr(x,y) = \frac{cov(x,y)}{\sigma_x \sigma_y} = \frac{E[(x-\bar{x})(y-\bar{y})]}{\sigma_x \sigma_y} \quad (6)$$

In general, all correlation coefficients are very small, indicating that there is a complex nonlinear relationship between the magnetic properties and composition of La-Co SrM. Compared with the relatively strong correlation between the H_{cJ} and each variable, all the correlation of the M_S is very weak. This also reveals that the method of increasing the saturation magnetization by ions substitution is difficult to control.

From the perspective of each composition, first, the Fe/Sr ratio has an obvious effect on the magnetic properties of strontium ferrite. Studies have shown that the iron-deficiency formula can cause vacancies in the

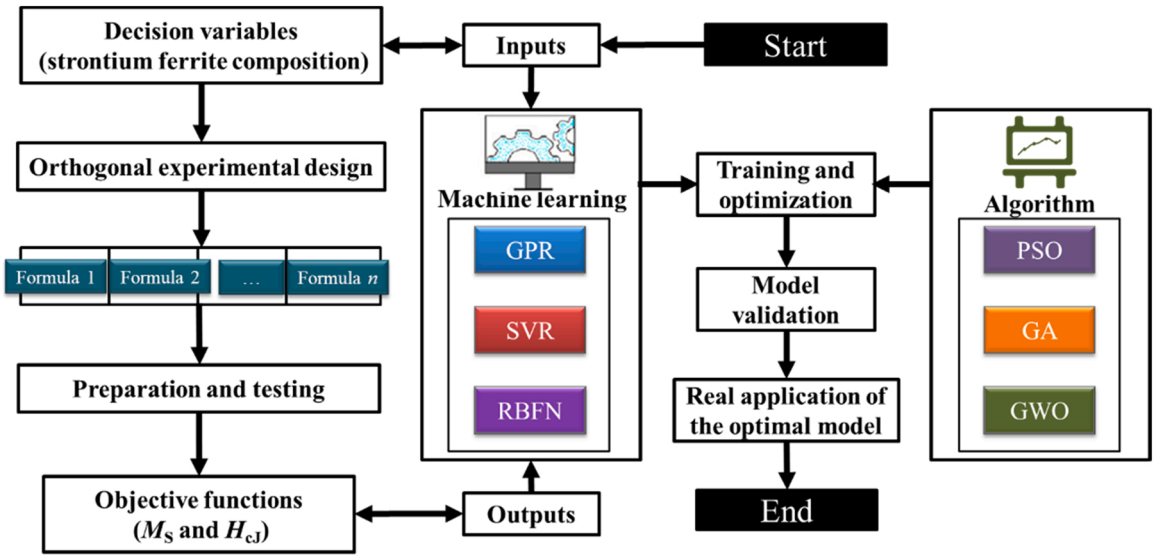

Fig. 9. Machine learning process of this work.

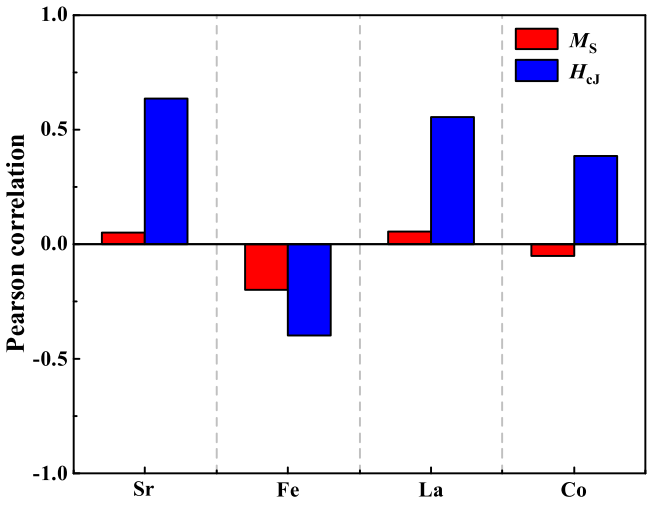

Fig. 10. Pearson correlation histogram of four independent variables (content of Sr, Fe, La, and Co) and two dependent variables (M_s and H_{cJ}): the red represents M_s; the blue represents H_{cJ}.

crystal structure [30–32]. On the one hand, the appearance of these vacancies facilitates the migration of ions during the sintering process and promotes the progress of the solid-state reaction, thereby generating more M-phase and promoting the compactness of the sample. On the other hand, the design of iron-deficiency formula can effectively suppress the appearance of non-magnetic miscellaneous α-Fe_2O_3 caused by excess Fe, and at the same time, SrO may be produced at the grain boundary, which can effectively inhibit the growth of grains, thereby significantly improving the H_{cJ} of the material. Therefore, when the Fe/Sr ratio is less than 12, it is more conducive to high H_{cJ}. Secondly, when the rare earth element La^{3+} ions replace Sr^{2+} in strontium ferrite, it can be known from the principle of electricity price balance that the corresponding equivalent amount of Fe^{3+} in 2*a* and $4f_2$ will become Fe^{2+} [33]. The change in valence increases the exchange coupling between Fe^{3+}—O^2—Fe^{3+} at 12*k*, so that the M_S gradually improves with the increase of La^{3+} concentration; and the anisotropy of Fe^{2+} is larger than Fe^{3+}, causing H_{cJ} increases. As the amount of single ion Co substitution increases, the M_S decreases mainly because that Co occupies a certain proportion of 2*a* and 12*k* positions, and the ionic magnetic moment of Co^{2+} is 3 μ_B, which is less than that of Fe^{3+}. The total effect is that the molecular magnetic moment in the spin-up direction is reduced, so the M_S decreases, and after the energy level of Co^{2+} splits in the crystal field, the orbital angular momentum is not completely "frozen", being a stronger anisotropy than Fe^{3+} [34].

3.2. Comparison and verification of machine learning models

To validate the accuracy of the machine learning models and the reliability of the experimental data simultaneously, the 20 sets of data under the related experimental conditions obtained from works of literature [35–37] were applied as a validation set. As Fig. 11 shows, the 20 sets of data are also sintered in solid-state reaction for La-Co substitution and contain M_S and H_{cJ} performance parameters. The main statistic parameters of the experiment training sets and literature testing sets are shown in Table 6.

The accuracy of a prediction model needs to be evaluated. In this paper, four frequently-used metrics namely, mean absolute error (MAE), mean relative error (MRE), root mean squared error (RMSE), and R-squared (R^2) were adopted to test whether the models are feasible. Meanwhile, the specific formula of these four metrics can be found in the reference [38].

The 4 quality metrics of the nine combinations for M_S are shown in Fig. 12. It is known that the more accurate the prediction, the more the point will be along with the forty-five-degree diagonal distribution. Obviously, the SVR-GWA model performs better than the other 8 models on the prediction of M_S. More specific, the MAE, MRE, RMSE, and R^2 are 0.50, 0.72 %, 0.56, and 0.9919, respectively. The MAE, MRE, and RMSE are small enough while the R^2 is close enough to 1 which means the SVR-GWA method meets the requirements evaluation accuracy. As for the H_{cJ}, it can be intuitively seen from Fig. 13 that the prediction results of the SVR-GWA method were closer to the forty-five-degree slope line. For more quantitative analysis, the MAE, MRE, RMSE, and R^2 of the SVR-GWA method are 0.1049, 3.21 %, 0.1201, and 0.9818, respectively. That is to say, the combination of the SVR model and GWA algorithm is more suitable for this type of problem.

3.3. Composition design of La-Co SrM

Now two accurate prediction models for M_S and H_{cJ} have been constructed. They can build a property prediction dataset in an arbitrary rational composition space with one or more dimensions, such as the variables in ***X***. We use the selected optimal model SVR-GWA to predict 2201 points in the component space and drew the contour map as shown

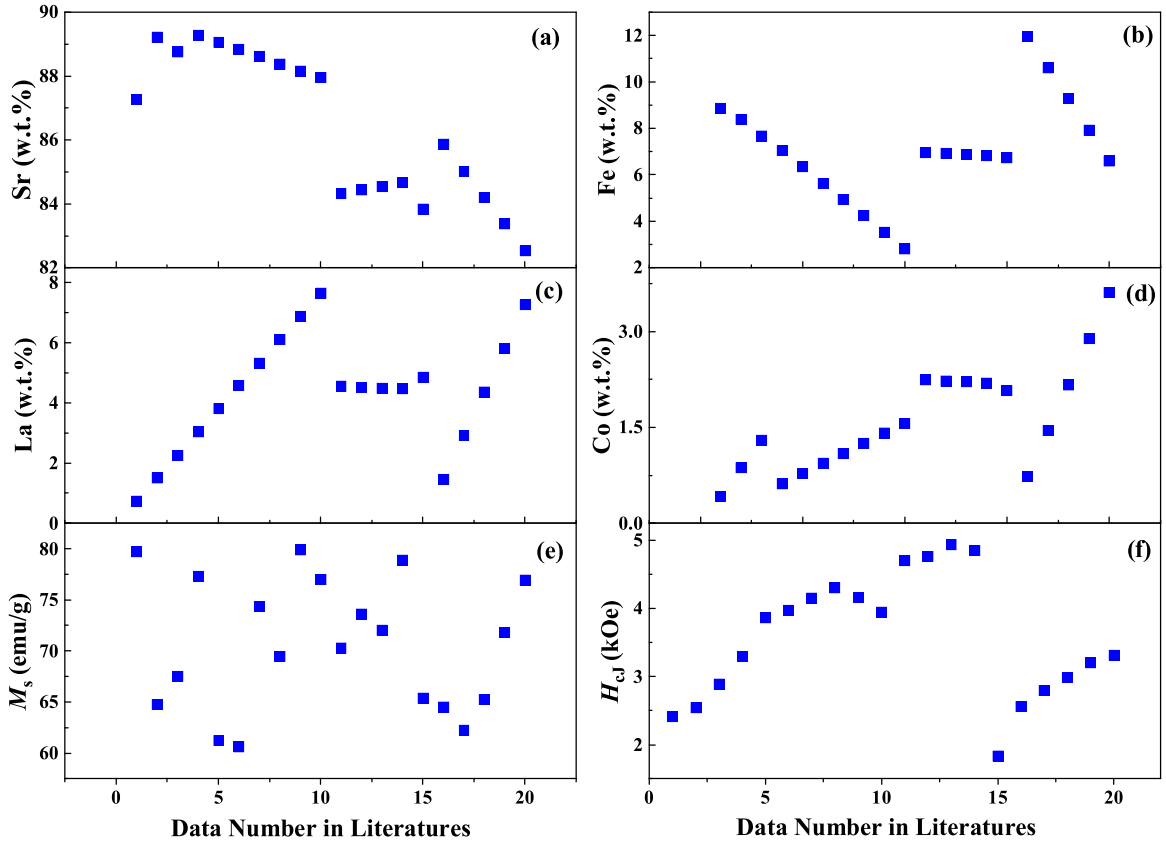

Fig. 11. The statistic of compositions (Sr, Fe, La, and Co) and magnetic properties (*Ms* and H_{cJ}) of 20 La-Co substitution Sr-hexaferrite from literature [35–37] for validating the accuracy of models: (a) content of Sr; (b) content of Fe; (c) content of La; (d) content of Co; (e) M_S; (f) H_{cJ}.

Table 6
The main statistic parameters of training and testing sets.

Index	Training set (145)						Testing set (20)					
	Sr	Fe	La	Co	M_S	H_{cJ}	Sr	Fe	La	Co	M_S	H_{cJ}
Min value	1.42	77.85	0	0	43.72	1.55	2.83	82.54	0.74	0.42	60.64	1.84
Max value	13.59	86.71	9.95	3.37	89.24	5.46	11.95	89.29	7.66	3.61	79.89	4.94
Mean value	8.08	82.17	4.97	1.64	72.59	3.61	7.01	86.42	4.33	1.60	70.66	3.58
STD	4.10	2.69	3.23	0.97	5.96	1.09	2.16	2.26	1.88	0.81	6.26	0.89

in Fig. 14, from which we can obtain corresponding M_S and H_{cJ} of the $Sr_{16-x}La_xFe_{84-y}Co_y$-O (*x* and *y* are mass fractions) ferrite with the mass fraction of cobalt oxide as x and the mass fraction of lanthanum oxide as y. The dotted lines in the figure represent the contour lines of each performance. The warmer the color, the higher the performance. These two prediction graphs show that there is almost no intersection between the highest points of the two performances, reflecting that M_S and H_{cJ} cannot reach the maximum at the same time, which is in line with our perception and can be proved by the Eq. (7) [39] that M_S and H_{cJ} are inversely proportional:

$$H_{cJ} = \frac{2K}{\mu_0 M_S} \tag{7}$$

where *K* is the magnetocrystalline anisotropy constant and μ_0 is the universal constant of permeability in free space, $4\pi \times 10^{-7}$ H/m.

However, we can adjust the La-Co composition to focus on a certain performance according to the actual situation. Otherwise, we can easily find high magnetic properties and realize composition design quickly in the prediction map. For example, as Fig. 15(a) shows, the blue area represents the region of high H_{cJ} with moderate M_S ($H_{cJ} \geq 5.0$ kOe and $M_S \geq 70$ emu/g). Similarly, the red area is the region of high M_S with $M_S \geq 80$ emu/g and $H_{cJ} \geq 4.0$ kOe. To further validate the accuracy of the prediction model, the Latin hypercube sampling (LHS) [40] method was adopted to randomly generate five representative samples from Fig. 15 (a) for experimental validation. Using the high M_S and high H_{cJ} regions as the demarcation, five points were labeled as numbers 1–5 in the direction of increasing La concentration *x* as shown in Fig. 15(a), which avoided all compositions of the training and validation sets. The La-Co SrM samples represented by the five points were prepared with the same process and their magnetic hysteresis lines were measured at room temperature as shown in Fig. 15(b). The substitution molar amounts of La and Co for the five samples, as well as the measured and predicted M_S and H_{cJ}, and calculated magnetic energy product $(BH)_{max}$ are summarized in Table 7. The experimental and predicted values of these five samples were plotted against the sample number in Fig. 15(c), which are very close to each other. And the accuracy evaluation indexes were also counted and shown in Fig. 15(c), where the MAE, MRE, RMSE, and R^2 of M_S are 0.4, 0.52 %, 0.42, and 0.995, respectively. Meanwhile, the four indexes of H_{cJ} are 0.068, 1.48 %, 0.084, and 0.983, respectively, which are similar to that of the testing set. Although the sample size of experimental validation is small, it fully reflects the accuracy of the prediction model.

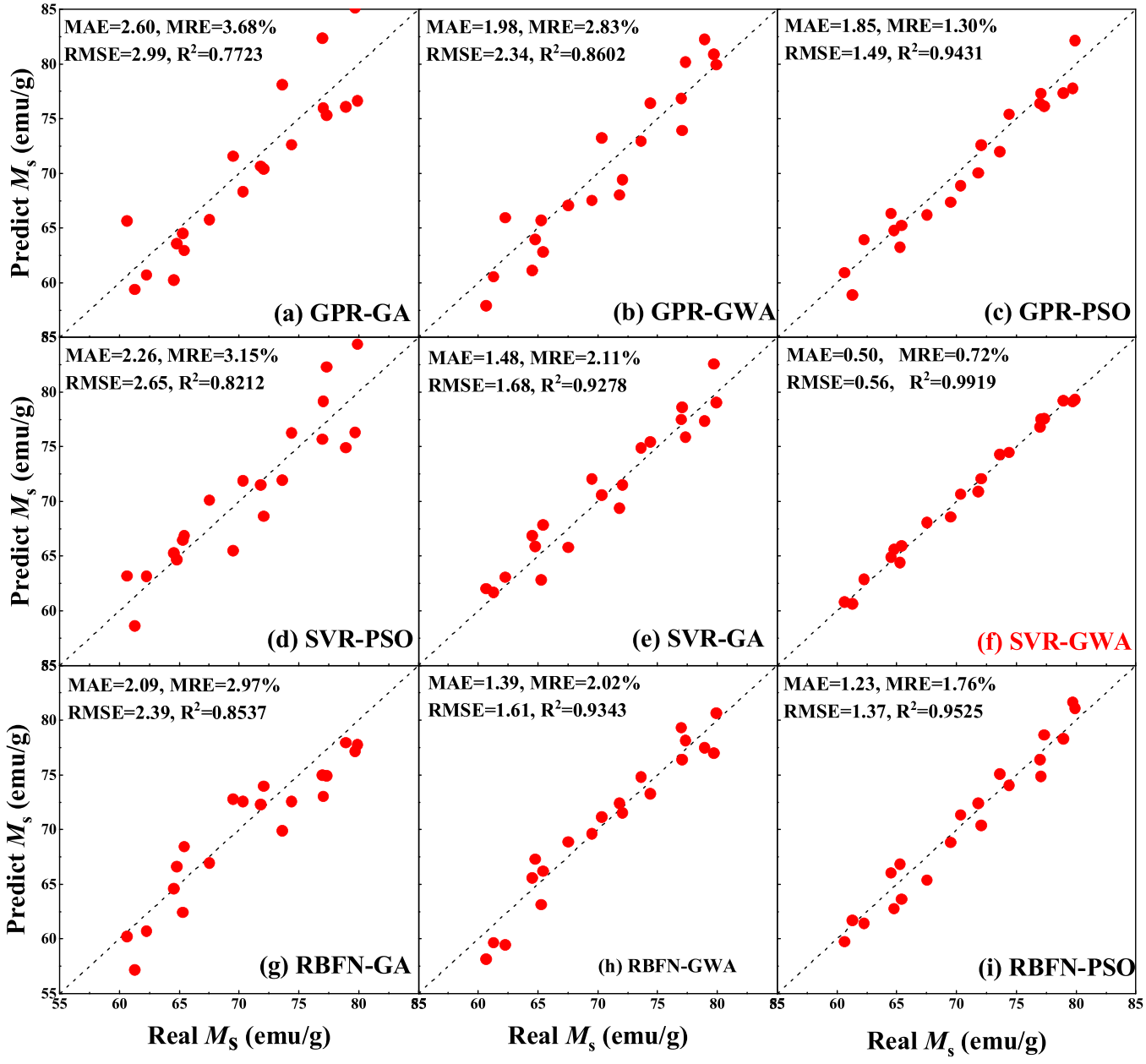

Fig. 12. Testing results of M_s by the 9 methods: the horizon axis represents the true values, and the vertical axis represents the predicted values by the corresponding models. The SVR-GWA model marked in red has the best prediction effect, and its R^2 reaches 0.9919.

According to the variation of magnetic properties with sample number, i.e., La concentration *x*, shown in Fig. 15(c) that to obtain high M_S, the concentration of Co is larger than that of La, because the Co ions with a smaller magnetic moment (3 μ_B) mainly occupy the spin-down sites of hexaferrite and increase the net total magnetic moment [41]. On the contrary, the magnetic anisotropy is further increased due to Fe^{2+} by charge compensation mechanism when La concentration is larger than Co [42], resulting in higher H_{cJ}. Furthermore, after comparing the $(BH)_{max}$ of five samples, sample No.4 with medium M_S and H_{cJ} performed the best. This means that we can choose the composition range reasonably according to actual demand. However, the factors affecting the magnetic properties are complex, especially second phases, defects, grain boundaries, etc. in polycrystalline samples. More characteristic parameters are needed for in-depth research on materials under wider process conditions. There is still a long way to go in machine learning research in the field of permanent ferrites.

4. Conclusion

In this study, a fast and accurate prediction of magnetic properties and composition design model for La-Co SrM was established based on high-through experiments, machine learning (ML) models, and nature-inspired algorithms. To screen out the most suitable method for the composition designing method of La-Co substitution, comparative research with 9 methods composed of 3 ML models and 3 algorithms were trained and validated with 145 samples obtained by high-throughput experimental and 20 data from the literature, respectively. It is concluded that the SVR-GWA method can predict both the M_S and H_{cJ} more accurately than the other 8 methods. In detail, in the SVR-GWA method the 4 quality metrics MAE, MRE, RMSE, and R^2 of the M_S are 0.50, 0.72 %, 0.56, and 0.9919, while 0.1049, 3.21 %, 0.1201, and 0.9818 for H_{cJ}.

Furthermore, the magnetic properties of $Sr_{1-x}La_xFe_{12-y}Co_yO19$ ferrite were predicted by the SVR-GWA method, from which, the influence of

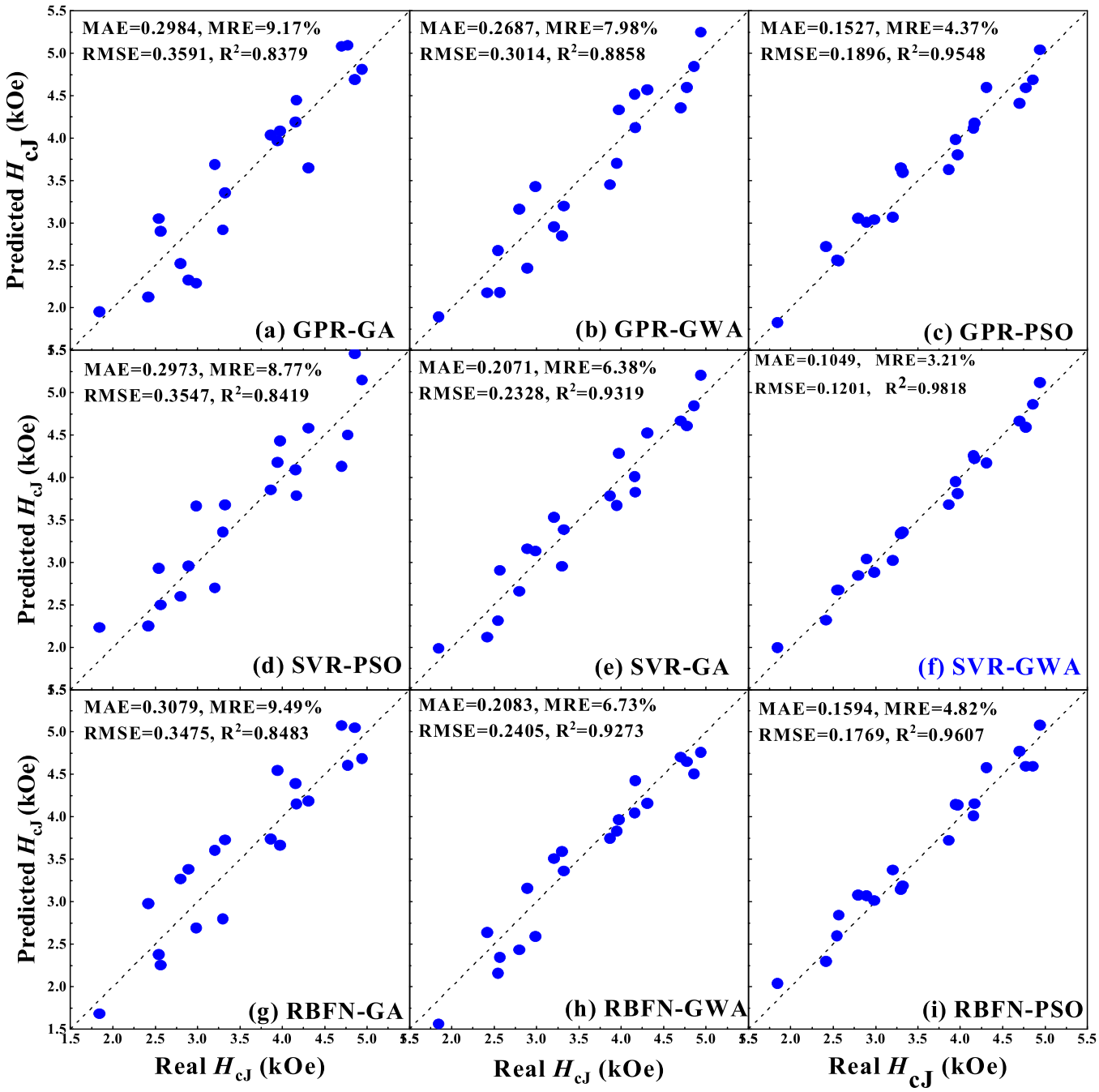

Fig. 13. Testing results of H_{cJ} by the 9 methods: the horizon axis represents the true values, and the vertical axis represents the predicted values by the corresponding models. The SVR-GWA model marked in blue has the best prediction effect, and its R^2 reaches 0.9818.

La-Co substitution on the two magnetic properties M_S and H_{cJ} of Sr-hexaferrite can be intuitively understood. The predicted results can be used as a reference for the efficient composition design of La-Co SrM. It is indicated that obtaining the composition with high M_S and H_{cJ} simultaneously is difficult, but we can realize position design from the prediction figure based on the actual demand. In general, when La concentration x is smaller than Co concentration y within $x \leq 0.3$, the M_S will be enhanced; otherwise, as x increases and is larger than y in the maximum substitution limit, the improved M_S would be obtained, but the samples with moderate M_S and H_{cJ} may have a larger magnetic energy product $(BH)_{max}$.

The above results have shown that the ML model could be a powerful method to quickly identify promising candidate strontium ferrite with target magnetic properties. And the reliability and applicability of the SVR-GWA method for the composition design of La-Co SrM have also been proved, which can also be applied to other materials with sufficient experimental data. It is worth noting that we merely took the La-Co SrM at the temperature of 1250 ℃ as an example due to the time-consuming experiment. Furthermore, we will add more process and microstructure parameters as the control variable in the prediction model to improve the practicability of the machine learning method and help the development of permanent magnets in the future.

CRediT authorship contribution statement

Ruoshui Liu (First Author): Conceptualization, Investigation, Methodology, Data curation, Formal analysis, Software, Formal analysis, Validation, Writing - Original Draft;**Lichen Wang:** Investigation,

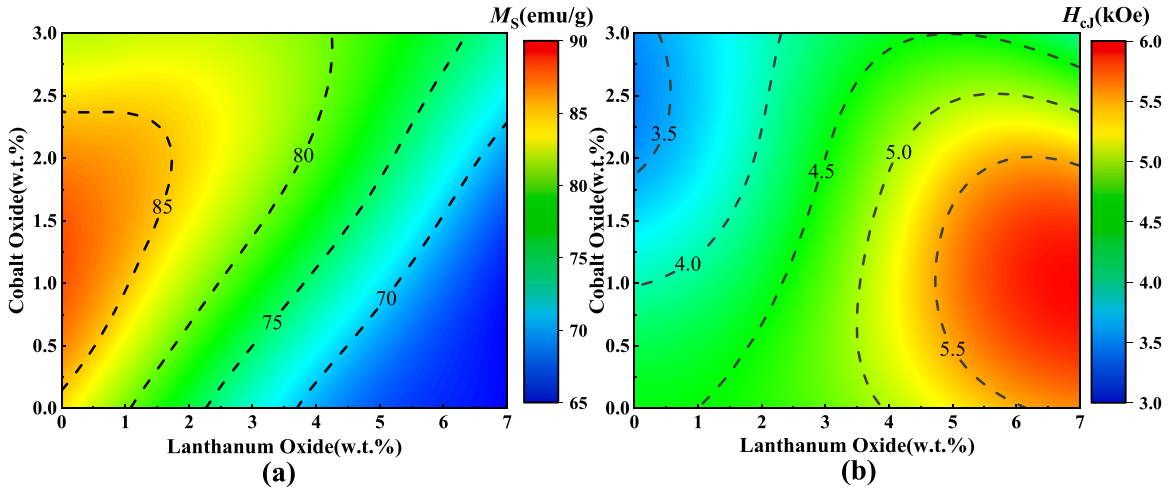

Fig. 14. Prediction maps of (a) M_S and (b) H_{cJ} by SVR-GWA for $Sr_{16-x}La_xFe_{84-y}Co_y$-O ($x$ and y are mass fractions) ferrite: the horizon axis represents the content of lanthanum oxide, and the vertical axis represents the content of cobalt oxide of raw materials. The warmer the color is, the higher the corresponding magnetic properties are. And the dotted line is the contour line, which means the magnetic properties are the same in this line.

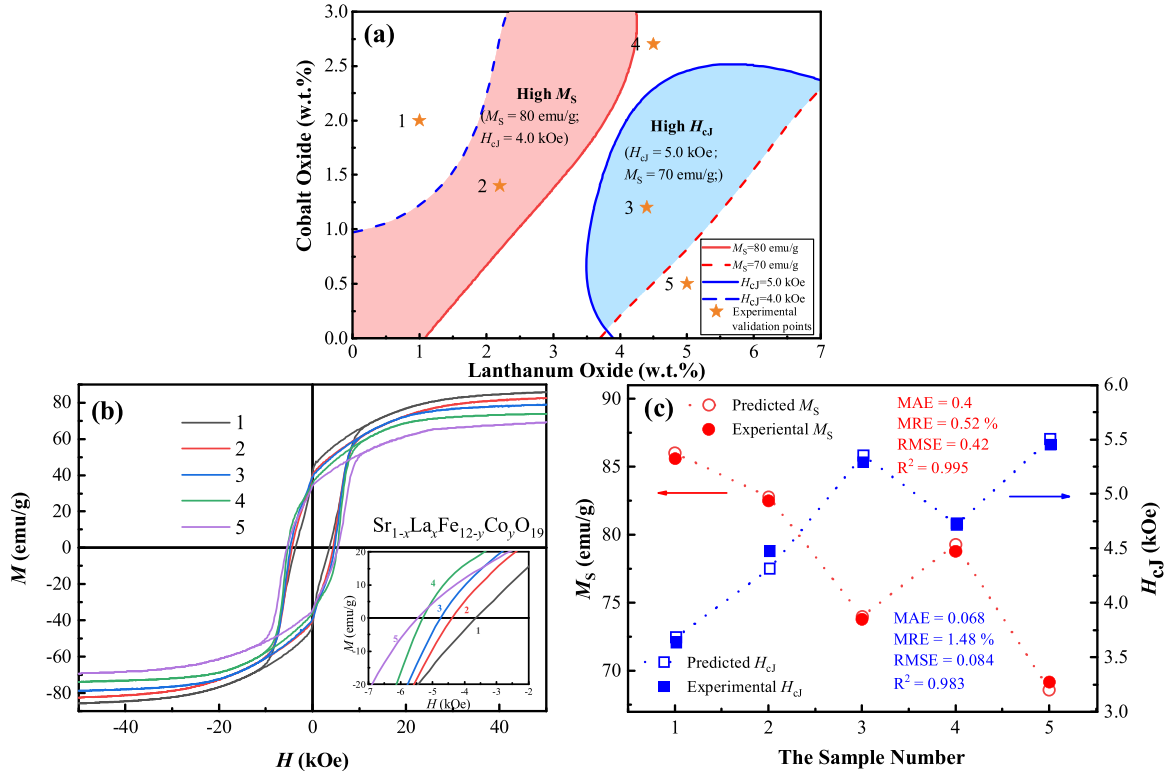

Fig. 15. (a) La-Co substitution range of high magnetic properties region. The blue and red regions represent the high H_{cJ} and high M_S, respectively. And the five orange star symbols were chosen for experimental validation. (b) The room temperature magnetic hysteresis lines for the five experimental validated samples with the inset of an enlargement of the demagnetization curves. (c) Measured and predicted M_S and H_{cJ} as a function of sample numbers with accuracy evaluation indexes.

Table 7
The La-Co composition, experimental and predicted M_S and H_{cJ} as well as $(BH)_{max}$ of the five $Sr_{1-x}La_xFe_{12-y}Co_yO_{19}$ samples.

NO.	x	y	M_S (emu/g)		H_{cJ} (kOe)		$(BH)_{max}$ (MGOe)
			Experiment	Predicted	Experiment	Predicted	
1	0.066	0.258	85.6	86.0	3.637	3.682	0.889
2	0.145	0.180	82.5	82.8	4.477	4.314	1.366
3	0.290	0.155	73.8	74.0	5.293	5.357	1.609
4	0.297	0.348	78.8	79.3	4.731	4.717	1.934
5	0.330	0.064	69.2	68.6	5.456	5.508	1.529

Writing – review & editing;**Zhiyi Xu:** – review & editing;**Ciyu Qin:** Investigation;**Ziyu Li:** Investigation;**Xiang Yu:** Investigation;**Dan Liu** : Writing – review & editing;**Huayang Gong:** Investigation;**Tongyun Zhao:** Project administration, Supervision;**Jirong Sun:** Resources, Funding acquisition;**Fengxia Hu:** Resources, Funding acquisition;**Baogen Shen (Corresponding Author):** Conceptualization, Funding acquisition, Resources, Supervision, Writing – review & editing.

Declaration of Competing Interest

The authors declare that they have no known competing financial interests or personal relationships that could have appeared to influence the work reported in this paper.

Data availability

Data will be made available on request.

Acknowledgments

This work was supported by the Science Center of the National Science Foundation of China (52088101), the National Key Research and Development Program of China (2021YFB3501202, 2020YFA0711502, 2019YFA0704900, 2018YFA0305704), the National Natural Sciences Foundation of China (U1832219, 51971240, 52101228, 52001012), the Strategic Priority Research Program B (XDB33030200), Beijing Natural Science Foundation (2214070) and the Key program of the Chinese Academy of Sciences (ZDRW-CN-2021–3).

References

[1] J.J. Went, G.W. Rathenau, E.W. Gorter, G.W.V. Oosterhout, Ferroxdure, a class of new permanent magnet materials, Philips Tech. Rev. 13 (1952) 194–208.
[2] R.C. Pullar, Hexagonal ferrites: a review of the synthesis, properties and applications of hexaferrite ceramics, Prog. Mater. Sci. 57 (2012) 1191–1334, https://doi.org/10.1016/j.pmatsci.2012.04.001.
[3] M.F. de Campos, D. Rodrigues, High technology applications of barium and strontium ferrite magnets, Mater. Sci. Forum 881 (2016) 134–139, https://doi.org/10.4028/www.scientific.net/MSF.881.134.
[4] K. Iida, Y. Minachi, K. Masuzawa, M. Kawakami, H. Nishio, H. Taguchi, High - performance ferrite magnets: M - Type Sr - ferrite containing lanthanum and cobalt, J. Magn. Soc. Jpn. 23 (1999) 1093–1096, https://doi.org/10.3379/jmsjmag.23.1093.
[5] Hitachi catalogue. ⟨http://www.hitachi-metals.co.jp/e/products/auto/el/p03_05.html⟩.
[6] TDK Ferrite Magnets Catalog. ⟨https://product.tdk.com/en/products/magnet/magnet/ferrite/index.html⟩.
[7] Z. Chen, F. Wang, S. Yan, Z. Feng, Microstructure and magnetic properties of M-type Sr0.61−xLa0.39CaxFe11.7Co0.3O19 hexaferrite prepared by microwave calcination, Mater. Sci. Eng.: B 182 (2014) 69–73, https://doi.org/10.1016/j.mseb.2013.11.027.
[8] Z. Chen, F. Wang, S. Yan, Y. Nie, Z. Feng, Y. Chen, V.G. Harris, Enhanced coercivity of CaLaCo-doped SrM hexaferrites by microwave-calcination technique, J. Am. Ceram. Soc. 97 (2014) 1873–1877, https://doi.org/10.1111/jace.12862.
[9] X. Huang, X. Liu, Y. Yang, K. Huang, X. Niu, D. Jin, S. Gao, Y. Ma, F. Huang, F. Lv, S. Feng, Microstructure and magnetic properties of Ca-substituted M-type SrLaCo hexagonal ferrites, J. Magn. Magn. Mater. 378 (2015) 424–428, https://doi.org/10.1016/j.jmmm.2014.09.049.
[10] Y. Yang, F. Wang, J. Shao, D. Huang, X. Liu, S. Feng, C. Wen, The impact of Co/La ratios on microstructure and magnetic properties of the Sr0.75−xCa0.25LaxFe12−yCoyO19 hexaferrites, J. Magn. Magn. Mater. 384 (2015) 64–69, https://doi.org/10.1016/j.jmmm.2015.02.016.
[11] F. Kools, A. Morel, R. Grössinger, J.M. Le Breton, P. Tenaud, LaCo-substituted ferrite magnets, a new class of high-grade ceramic magnets; intrinsic and microstructural aspects, J. Magn. Magn. Mater. 342–245 (2002) 1270–1276, https://doi.org/10.1016/S0304-8853(01)00988-X.
[12] R. Grössinger, C. Tellez Blanco, M. Küpferling, M. Müller, G. Wiesinger, Magnetic properties of a new family of rare-earth substituted ferrites, Phys. B: Condens. Matter 327 (2003) 202–207, https://doi.org/10.1016/s0921-4526(02)01728-3.
[13] A. Razek, M. Tyrman, A. Pasko, O. De La Barrière, F. Mazaleyrat, Structural and magnetic properties of an anisotropic M-type LaCo-substituted strontium hexaferrite, Eur. Phys. J. Appl. Phys. 72 (2015), https://doi.org/10.1051/epjap/2015150099.
[14] D.H. Choi, S.W. Lee, I.-B. Shim, C.S. Kim, Mössbauer studies for La–Co substituted strontium ferrite, J. Magn. Magn. Mater. 304 (2006) e243–e245, https://doi.org/10.1016/j.jmmm.2006.01.151.
[15] A. Morel, J.M. Le Breton, J. Kreisel, G. Wiesinger, F. Kools, P. Tenaud, Sublattice occupation in Sr1−xLaxFe12−xCoxO19 hexagonal ferrite analyzed by Mössbauer spectrometry and Raman spectroscopy, J. Magn. Magn. Mater. 342–245 (2002) 1405–1407, https://doi.org/10.1016/s0304-8853(01)00962-3.
[16] N. Nagasawa, M. Oura, S. Ikeda, T. Waki, Y. Tabata, H. Nakamura, H. Kobayashi, Magnetic anisotropies of La–Co substituted M-type Sr hexaferrites studied by 57Fe Mössbauer spectroscopy with external magnetic fields, J. Appl. Phys. 128 (2020), https://doi.org/10.1063/5.0019954.
[17] H. Sakai, T. Hattori, Y. Tokunaga, S. Kambe, H. Ueda, Y. Tanioku, C. Michioka, K. Yoshimura, K. Takao, A. Shimoda, T. Waki, Y. Tabata, H. Nakamura, Occupation sites and valence states of Co dopants in (La, Co)-codoped M-type Sr ferrite: 57Fe and 59Co nuclear magnetic resonance studies, Phys. Rev. B 98 (2018), https://doi.org/10.1103/PhysRevB.98.064403.
[18] A. Agrawal, A. Choudhary, Perspective: materials informatics and big data: realization of the “fourth paradigm” of science in materials science, APL Mater. 4 (2016), https://doi.org/10.1063/1.4946894.
[19] I. Kucuk, H. Sözeri, H. Özkan, Modeling of magnetic properties of nanocrystalline La-doped barium hexaferrite, J. Supercond. Nov. Magn. 24 (2010) 1333–1337, https://doi.org/10.1007/s10948-010-0828-3.
[20] H. Sozeri, I. Kucuk, H. Ozkan, Phase identification of la-doped hard magnetic barium ferrite using artificial neural network, J. Supercond. Nov. Magn. 24 (2010) 683–687, https://doi.org/10.1007/s10948-010-0937-z.
[21] T. Pourashraf, S. Shokri, M. Yousefi, A. Ahmadi, P.A. Azar, Implementing Machine Learning in Laboratory Synthesis by Hybrid of SVR Model and Optimization Algorithms, Adv. Theory Simul. 4 (2021), https://doi.org/10.1002/adts.202100225.
[22] M.L. Green, C.L. Choi, J.R. Hattrick-Simpers, A.M. Joshi, I. Takeuchi, S.C. Barron, E. Campo, T. Chiang, S. Empedocles, J.M. Gregoire, A.G. Kusne, J. Martin, A. Mehta, K. Persson, Z. Trautt, J. Van Duren, A. Zakutayev, Fulfilling the promise of the materials genome initiative with high-throughput experimental methodologies, Appl. Phys. Rev. 4 (2017), https://doi.org/10.1063/1.4977487.
[23] M. Seeger, Gaussian processes for machine learning, Int. J. Neural Syst. 14 (2004) 69, https://doi.org/10.1142/S0129065704001899.
[24] L. Wang, Y. Yao, K. Wang, C.D. Adenutsi, G. Zhao, F. Lai, Hybrid application of unsupervised and supervised learning in forecasting absolute open flow potential for shale gas reservoirs, Energy, DOI 10.1016/j.energy.2021.122747(2021) 122747. https://doi.org/10.1016/j.energy.2021.122747.
[25] H. Yu, Y. Tan, J. Zeng, C. Sun, Y. Jin, Surrogate-assisted hierarchical particle swarm optimization, Inf. Sci. 454 (2018) 59–72, https://doi.org/10.1016/j.ins.2018.04.062.
[26] R. Eberhart, J. Kennedy, A new optimizer using particle swarm theory, MHS'95. Proceedings of the Sixth International Symposium on Micro Machine and Human Science, Ieee, 1995, pp. 39–43.
[27] S. Katoch, S.S. Chauhan, V. Kumar, A review on genetic algorithm: past, present, and future, Multimed. Tools Appl. 80 (2021) 8091–8126, https://doi.org/10.1007/s11042-020-10139-6.
[28] S. Mirjalili, S.M. Mirjalili, A. Lewis, Grey wolf optimizer, Adv. Eng. Softw. 69 (2014) 46–61, https://doi.org/10.1016/j.advengsoft.2013.12.007.
[29] J. Lee Rodgers, W.A. Nicewander, Thirteen ways to look at the correlation coefficient, Am. Stat. 42 (1988) 59–66.
[30] A. Vijayalakshmi, N.S. Gajbhiye, Magnetic properties of single-domain SrFe12O19 particles synthesized by citrate precursor technique, J. Appl. Phys. 83 (1998) 400–406, https://doi.org/10.1063/1.366654.
[31] Y.P. Fu, C.H. Lin, Fe/Sr ratio effect on magnetic properties of strontium ferrite powders synthesized microwave-induced combustion process, J. Alloy. Compd. 386 (2005) 222–227, https://doi.org/10.1016/j.jallcom.2004.04.148.
[32] M. Jean, V. Nachbaur, J. Bran, J.M.Le Breton, Synthesis and characterization of SrFe12O19 powder obtained by hydrothermal process, J. Alloy. Compd. 496 (2010) 306–312, https://doi.org/10.1016/j.jallcom.2010.02.002.
[33] S. Ounnunkad, Improving magnetic properties of barium hexaferrites by La or Pr substitution, Solid State Commun. 138 (2006) 472–475, https://doi.org/10.1016/j.ssc.2006.03.020.
[34] Y. Ogata, Y. Kubota, T. Takami, M. Tokunaga, T. Shinokara, Improvements of magnetic properties of Sr ferrite magnets by substitutions of La and Co, IEEE Trans. Magn. 35 (1999) 3334–3336, https://doi.org/10.1109/20.800516.
[35] K.-S. Moon, E.-S. Lim, Y.-M. Kang, Effect of Ca and La substitution on the structure and magnetic properties of M-type Sr-hexaferrites, J. Alloy. Compd. 771 (2019) 350–355, https://doi.org/10.1016/j.jallcom.2018.08.306.
[36] Y. Yang, X. Liu, D. Jin, The impact of the iron content on the microstructure and magnetic properties of M-type ferrites Sr0.45Ca0.25La0.30FexCo0.25O19, Mater. Sci. Eng.: B 186 (2014) 106–111, https://doi.org/10.1016/j.mseb.2014.03.005.
[37] Y. Yang, X. Liu, D. Jin, Y. Ma, Structural and magnetic properties of La–Co substituted Sr–Ca hexaferrites synthesized by the solid state reaction method, Mater. Res. Bull. 59 (2014) 37–41, https://doi.org/10.1016/j.materresbull.2014.06.003.
[38] L. Wang, Z.P. Li, C.D. Adenutsi, L. Zhang, F.P. Lai, K.J. Wang, A novel multi-objective optimization method for well control parameters based on PSO-LSSVR proxy model and NSGA-II algorithm, J. Pet. Sci. Eng. 196 (2021), https://doi.org/10.1016/j.petrol.2020.107694.
[39] E. Gorter, Saturation magnetization of some ferrimagnetic oxides with hexagonal crystal structures, Proceedings of the IEE-Part B: Radio and Electronic Engineering, 104 (1957) 255–260.

[40] M. Stein, Large sample properties of simulations using Latin hypercube sampling [J], Technometrics 29 (2) (1987) 143–151, https://doi.org/10.1080/00401706.1987.10488205.
[41] A. Shimoda, K. Takao, K. Uji, T. Waki, Y. Tabata, H. Nakamura, Flux growth of magnetoplumbite-type strontium ferrite single crystals with La–Co co-substitution, J. Solid State Chem. 239 (2016) 153–158, https://doi.org/10.1016/j.jssc.2016.04.031.
[42] H. Ueda, Y. Tanioku, C. Michioka, K. Yoshimura, Magnetocrystalline anisotropy of La- and Co-substituted M-type strontium ferrites: Role of Co2+ and Fe2+, Phys. Rev. B 95 (2017) https://doi.org/10.1103/PhysRevB.95.224421.